Final Draft
of the original manuscript:

Gizer, G.; Puszkiel, J.; Cao, H.; Pistidda, C.; Le, T.; Dornheim, M.; Klassen, T.:
Tuning the reaction mechanism and hydrogenation/dehydrogenation properties of 6Mg(NH2)2single bond9LiH system by adding LiBH4.
In: International Journal of Hydrogen Energy. Vol. 44 (2019) 23, 11920 - 11929.
First published online by Elsevier: 11.04.2019

https://dx.doi.org/10.1016/j.ijhydene.2019.03.133

Tuning the reaction mechanism and hydrogenation/dehydrogenation properties of $6Mg(NH_2)_2$-9LiH system by adding $LiBH_4$

Gökhan Gizer,[a] *Julián Puszkiel,*[a,b] *Hujun Cao,*[a] *Claudio Pistidda,*[*a] *Thi Thu Le,*[a] *Martin Dornheim,*[*a] *Thomas Klassen* [a,c]

[a] Department of Nanotechnology, Institute of Materials Research, Helmholtz–Zentrum Geesthacht, Max-Planck-Straße 1, 21502 Geesthacht, Germany

[b] Department of Physicochemistry of Materials, Consejo Nacional de Investigaciones Científicas y Técnicas (CONICET), Centro Atómico Bariloche, Av. Bustillo km 9500, S.C. de Bariloche, Argentina.

[c] Helmut Schmidt University, Holstenhofweg 85, 22043 Hamburg, Germany

Corresponding Authors

*E-mail: claudio.pistidda@hzg.de, martin.dornheim@hzg.de

Abstract

The hydrogen storage properties of $6Mg(NH_2)_2$-9LiH-$x(LiBH_4)$ (x = 0, 0.5, 1, 2) system and the role of $LiBH_4$ on the kinetic behaviour and the dehydrogenation/hydrogenation reaction mechanism were herein systematically investigated. Among the studied compositions, $6Mg(NH_2)_2$-9LiH-$2LiBH_4$ showed the best hydrogen storage properties. The presence of 2 mole of $LiBH_4$ improved the thermal behaviour of the $6Mg(NH_2)_2$-9LiH by lowering the dehydrogenation peak temperature nearly 25 °C and by reducing the apparent dehydrogenation activation energy of about 40 kJ/mol. Furthermore, this material exhibited fast dehydrogenation (~10 minutes) and hydrogenation kinetics (~ 3 minutes) and excellent cycling stability with a reversible hydrogen capacity of ~ 3.5 wt. % at isothermal 180 °C. Investigations on the reaction pathway indicated that the observed superior kinetic behaviour likely related to the formation of $Li_4(BH_4)(NH_2)_3$. Studies on the rate-limiting steps hinted that the sluggish kinetic behaviour of the $6Mg(NH_2)_2$-9LiH pristine material are attributed to an interface-controlled mechanism. On the contrary, $LiBH_4$-containing samples show a diffusion-controlled mechanism. During the first dehydrogenation reaction, the possible formation of $Li_4(BH_4)(NH_2)_3$ accelerates the reaction rates at the interface. Upon hydrogenation, this 'liquid like' of $Li_4(BH_4)(NH_2)_3$ phase assists the diffusion of small ions into the interfaces of the amide-hydride matrix.

Keywords: Solid-state hydrogen storage, Amide-Hydrides, Li-Mg-N-H system

1 Introduction

The uncontrolled release of greenhouse gases into the atmosphere threatens the future life of the humankind [1]. Regarding the emission of CO_2, in order to limit the average global temperature rise to maximum 2 °C, its quantity must be reduced of about 470 gig tons by 2050 [2]. In 2015, just 19.3 % of global electrical energy consumption was provided by renewable energy sources [3]. The share of renewable sources must rise to more than 60 % by 2050 to meet the '2 °C' goal [2]. To achieve this target, conventional fossil fuels must be replaced with alternative environmentally friendly fuels [4]. In this regard, hydrogen is an ideal fuel, since it has a gravimetric energy density (142 MJ/kg) 3 times higher than that of gasoline (46 MJ/kg), and its combustion leads to the production of H_2O only [5]. However, 1 kg of hydrogen has a volume of 11 m^3 [6]. To increase the volumetric energy density, hydrogen can be compressed, liquefied or chemically bonded. In the last decades, the possibility to store hydrogen into complex metal hydrides such as alanates, borohydrides and amides was thoroughly investigated [7–21]. Gay-Lussac and Thènard discovered amides such as sodium amide ($NaNH_2$) and potassium amide (KNH_2) in the beginning of 1800s [22]. Following this work, Dafert and Miklauz reported on the possibility to form a mixture of $LiNH_2$ and 2LiH from Li_3N with H_2 in 1910 [23]. Until few years ago, amides were not considered as a hydrogen storage material, since significant amount of ammonia gas were released during their thermal decomposition [24,25]. Amides started to be considered as a hydrogen storage medium for the first time in 2002, when Chen et al. reported that the $LiNH_2$ + LiH system could reversibly absorb/desorb ~ 6.5 wt. % of hydrogen according to reaction 1 [26];

$$Li_2NH + H_2 \leftrightharpoons LiNH_2 + LiH \qquad \Delta H = -45\ \text{kJ mol}^{-1} \qquad (1)$$

Temperatures higher than 250 °C are required to release hydrogen from $LiNH_2$ + LiH, thus this system is unsuitable for vehicular applications. Substituting the Li^+ cation with other alkaline and alkaline earth metal cations, several amide–hydride systems were discovered [27–30]. The system $Mg(NH_2)_2$ + 2LiH ($\Delta H = 40\ kJ\ mol^{-1}$) reversibly desorbs ~ 5.2 wt. % H_2 at 220 °C according to reactions 2 and 3 [28];

$$2Mg(NH_2)_2 + 3LiH \leftrightharpoons Li_2Mg_2(NH)_3 + LiNH_2 + 3H_2 \quad (2)$$

$$Li_2Mg_2\ (NH)_3 + LiNH_2 + LiH \leftrightharpoons 2Li_2Mg(NH)_2 + H_2 \quad (3)$$

Enormous efforts have been devoted to improve the kinetic behaviour and to reduce the reaction temperature of this system [31–35]. The addition of KH reduces the desorption peak temperature of Li-Mg-N-H system composed of $Mg(NH_2)_2$ and LiH from 180 °C to 132 °C [36,37]. Rb-containing materials have the same kinetic effects on this system [38]. Co-addition of Rb and K further improves the performance and enables achieving full desorption at 130 °C under vacuum conditions. In these cases, the catalytic species appears to be a solid solution of KH and RbH (i.e. K(Rb)H) [39]. Similar to K/Rb compounds, borohydrides; such as $Mg(BH_4)_2$ or $CaBH_4$ were also can reduce dehydrogenation temperatures and to enhance the desorption properties of Li-Mg-N-H system [40,41]. Previous reports revealed that both $Mg(BH_4)_2$ and $CaBH_4$ undergo metathesis reactions with LiH to form $LiBH_4$ and MgH_2 or CaH_2. $LiBH_4$ is the specie that improves the system performance and the formation of side products such as MgH_2 or CaH_2 reduces the reversible hydrogen capacity of the system. The addition of 0.1 mole $LiBH_4$ to $Mg(NH_2)_2$ + 2LiH not only improves the reaction kinetics, but also reduces the reaction enthalpy from 38.9 kJ/(mol H_2) to

36.5 kJ/(mol H_2) [42,43]. Thermodynamic alteration is achieved by stabilizing the dehydrogenation product, which refers to $LiNH_2$ in this system [44]. Depending on the molar ratios of $Mg(NH_2)_2$, LiH and $LiBH_4$; H_2 capacities and operating temperatures can be tailored [45]. $6Mg(NH_2)_2 + 9LiH + xLiBH_4$ (x = 0, 0.5, 1, 2) system offers theoretical H_2 capacities ranging between 4.0 to 4.5 wt. % at moderate temperatures (140 °C - 200 °C), based on the general reaction 4;

$$6Mg(NH_2)_2 + 9LiH + xLiBH_4 \leftrightharpoons 3Li_2Mg_2(NH)_3 + (LiNH_2)_3(LiBH_4)_x + 9H_2 \quad (4)$$

Varying $LiBH_4$ content, different dehydrogenation products can be obtained, i.e. $LiNH_2$, $Li_4(BH_4)(NH_2)_3$ or $Li_2(BH_4)(NH_2)$ [46]. The formation of complex amide-borohydrides ($Li_4(BH_4)(NH_2)_3$, $Li_2(BH_4)(NH_2)$) play a crucial role in improving the kinetic behaviour of the $6Mg(NH_2)_2 + 9LiH + xLiBH_4$ system [47]. Moreover, the complex amide-borohydride $Li_4(BH_4)(NH_2)_3$ is known to have a high ion conductivity and a melting point of ~190 °C [48]. In addition, the melting point of $Li_2(BH_4)(NH_2)$ is 90 °C and ion conductivity at its melting temperature is doubled respect to $Li_4(BH_4)(NH_2)_3$ [48].

Hitherto, a limited number of publications about the cycling properties of Li-Mg-B-N-H system composed of $Mg(NH_2)_2$, LiH and $LiBH_4$ are available in literatures [44,49–51]. Moreover, an exhaustive detailed investigation on the cycling and the kinetic behaviours of the $6Mg(NH_2)_2 + 9LiH + xLiBH_4$ has not been reported yet. In this work, we study different aspects of the hydrogen storage properties of the $6Mg(NH_2)_2 + 9LiH + xLiBH_4$ (x = 0, 0.5, 1, 2) system upon 20 dehydrogenation/hydrogenation cycles in a Sieverts apparatus. Thermal properties of the samples before and after cycling are investigated by Differential Scanning Calorimetry (DSC). Structural

properties are investigated with Powder X-Ray Diffraction (PXD) and Fourier transform Infrared Spectroscopy (FT-IR). Furthermore, it is herein performed an analysis about the dependence of reaction pathway and rate-limiting step on the amount of $LiBH_4$.

2 Experimental

The chemicals used in this work are MgH_2 (95 % purity, Rockwood Lithium GmbH), $LiBH_4$ (95 % purity, Sigma Aldrich) and LiH (97 % purity, Alfa Aesar). $Mg(NH_2)_2$ is synthesized in-house *via* two-step process. Firstly, MgH_2 was ball milled at 400 rpm under 7 bar of NH_3 for 24 hours. Each 6 hours, the gas in the milling vial was re-filled by pure NH_3. Milling procedure was performed in a Fritsch P6 planetary ball-milling device. Then, the collected sample was heated up to 310 °C under 7 bar of NH_3 in a high pressure vessel from Parr Instrument Company to optimize the yield of $Mg(NH_2)_2$. The purity of the obtained $Mg(NH_2)_2$ was characterized *via* thermogravimetric analysis (TG) (~95 % purity). $Mg(NH_2)_2$ was mixed with LiH and $LiBH_4$ in the molar ratios 6:9:0, 6:9:0.5, 6:9:1 and 6:9:2 by ball milling in a stainless steel high pressure milling vessel from Evico GmbH [52]. For the sake of clarity, all the samples are designated throughout the paper as shown in Table 1. Ball to powder ratio was 60:1. Milling processes were performed for 36 hours at a speed of 400 rpm. Before starting the milling processes, the milling vials were filled with 50 bar of H_2 to prevent possible H_2 release from the samples upon milling. The material preparation and handling were carried out in an argon-filled glove box (H_2O and O_2 levels below 10 ppm).

Table 1 − Compositions and designations for the investigated samples

Sample composition	Sample code
$6Mg(NH_2)_2 + 9LiH$	Mg-Li
$6Mg(NH_2)_2 + 9LiH + 0.5LiBH_4$	Mg-Li-0.5$LiBH_4$
$6Mg(NH_2)_2 + 9LiH + LiBH_4$	Mg-Li-1$LiBH_4$
$6Mg(NH_2)_2 + 9LiH + 2LiBH_4$	Mg-Li-2$LiBH_4$

Differential scanning calorimetry (DSC) measurements were performed in a Netzsch DSC 204 HP calorimeter located inside an argon-filled glovebox (H_2O and O_2 levels below 1 ppm). About 5 mg of each sample were placed in a Al_2O_3 crucible and then heated from room temperature to 300 °C with a heating rate of 3 °C/min. All measurements were done under 1 bar of H_2 backpressure. Before starting the measurement, the DSC chamber was first evacuated and then flushed 3 times with 10 bar of H_2. A mass flow-meter was used to maintain the hydrogen pressure in the range of 1 ± 0.2 bar of H_2 during heating up and cooling down.

In order to calculate apparent activation energies (E_a), many methods have been developed so far [53–56]. In this work, effects of additive on the kinetic behaviour of solid-gas reactions were calculated *via* Kissinger method, applying calorimetry [54]. This method is suitable for the samples that exhibit multi-step reactions and it allows us to determine E_a of a reaction process without assuming a kinetic model, i.e. without determining the rate limiting step of the reaction. The equation for the Ea calculation is shown in Eq. 5;

$$ln(\beta/T_m^2) = ln(AR/E_a) - \frac{E_a}{RT_m} \quad (5)$$

, where A is the pre-exponential factor and R is the gas constant. The temperature for the maximum reaction rate (T_m) was obtained from DSC curves measured at heating rates (β) of 1 °C/min, 3 °C/min, 5 °C/min and 10 °C/min under 1 bar of H_2 backpressure (ESI Figure 3). Then, $ln\left(\frac{\beta}{T_m^2}\right)$ against 1000/T_m was plotted, E_a and A was calculated from linear fitting.

Dehydrogenation/hydrogenation experiments were done using an in-house made Sieverts apparatus. About 70 mg of sample was used in each experiment. 20 dehydrogenation/hydrogenation cycles were performed at 180 °C under 1 bar and 80 bar of H_2, respectively. Due to the long measurement time necessary to achieve complete desorption and absorption (5 h for desorption and 8 h for absorption reactions), the Mg-Li sample was cycled only 10 times instead of 20.

In order to assess the rate-limiting steps of the dehydrogenation process in the studied system, Sharp and Jones method was applied [57, 58]. In this method, experimental data are expressed as following:

$$F(\alpha) = A\left(\frac{t}{t_{0.5}}\right) \quad (6)$$

, where A is the rate constant, $t_{0.5}$ is the time at the reaction fraction α = 0.5. The fraction (α) is taken as the hydrogen capacity over the maximum reached capacity for each sample. By implementing different rate equations, several plots of $(\frac{t}{t_{0.5}})_{\text{theoretical}}$ versus $(\frac{t}{t_{0.5}})_{\text{experimental}}$ are obtained. In this study, we applied this model to the portion of dehydrogenation curve between 0.1 and 0.8 fraction of the overall hydrogen capacity. We implemented 11 different rate equations as listed in ESI - Table S1. The best fitting reaction rate model must obey the following rules; slope of the fitted line should be ~ 1, intercept ~ 0 and R^2 ~ 1.

The composition of dehydrogenated samples was investigated by powder X-ray diffraction method (PXD) using a Bruker D8 Discover diffractometer equipped with Cu X-ray source (λ = 1.54184 Å) operating at 50 kV and 1000 mA and a 2D VANTEC detector. Diffraction patterns were collected in the angular range of 2θ range from 10 ° to 90 °. Information on the structural properties was taken from ICSD database [59]. A sample holder sealed with a poly(methyl methacrylate) (PMMA) dome was utilized to prevent the sample oxidation during PXD measurements.

Due to the possible presence of phases in the amorphous or monocrystalline state, the samples were also characterized *via* Fourier transform infrared technique (FT-IR). For this purpose, a Agilent Technologies Cary 630 FT-IR located in an argon filled glove box was used (H_2O and O_2 levels below 1 ppm). Each measurement was acquired in the spectral range of 650 cm^{-1} - 4000 cm^{-1} with a resolution of 4 cm^{-1}.

3 Results and Discussion

3.1 Thermal properties and activation energies

DSC curves of as-milled samples Mg-Li, Mg-Li-0.5$LiBH_4$, Mg-Li-1$LiBH_4$ and Mg-Li-2$LiBH_4$ measured at a heating ramp of 3 °C/min between room temperature and 300 °C are presented in Figure 1 (a). DSC curve of Mg-Li has two overlapping endothermic peaks with maxima at 197 °C and 205 °C ascribed to the two reaction steps described by eq. (2) and (3). In the samples containing $LiBH_4$, peak maxima are positioned at 191 °C and 180 °C for Mg-Li-0.5$LiBH_4$ and Mg-Li-1$LiBH_4$, respectively. Mg-Li-2$LiBH_4$ interestingly shows a single dehydrogenation peak at temperature of 176 °C, which is nearly 25 °C lower in respect to Mg-Li. The presence of a single

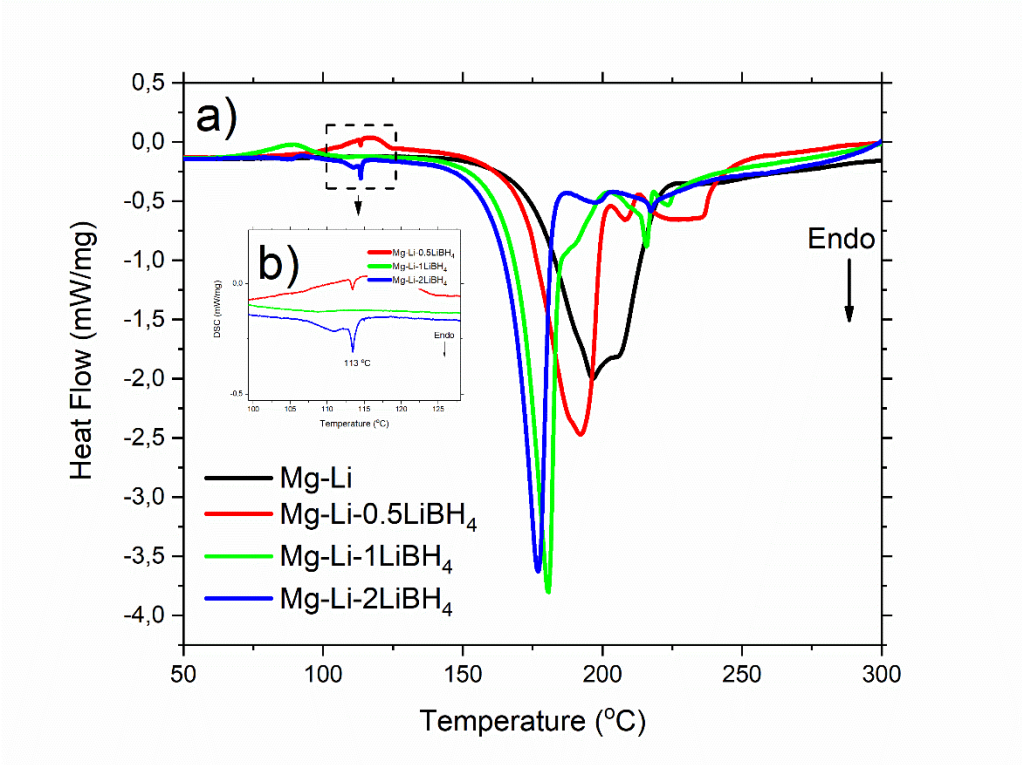

Figure 1 − (a) DSC curves of as-milled samples measured in the temperature range of 20 °C - 300 °C with a heating ramp of 3 °C /min and 1 bar of H_2 pressure (b) Phase transition of $LiBH_4$.

peak instead of two peaks, is most likely due to a change in the reaction pathway. All $LiBH_4$-containing samples present exothermic broad peaks between 75 °C and 125 °C, which most likely are caused by recrystallization of $LiBH_4$ on the $Mg(NH_2)_2$ [60]. Additionally, they have a small endothermic peak at 113 °C (Figure 1-b) which is ascribable to the phase transition of $LiBH_4$ from orthorhombic to hexagonal lattice structure [61]. However, this is not always visible as observed in the DSC curve of Mg-Li-1$LiBH_4$ (Figure 1). Additionally, based on the PXD analysis of the samples heat treated up to 300 °C, decomposition of $Li_4(BH_4)(NH_2)_3$ to Li_3BN_2 was observed (ESI: Figure S1). Non-isothermal measurements of the gas evolved during dehydrogenation measured in an Ar flow in the temperature range ~ 20 - 300 °C (ESI: Figure S2) show that the main released gas is hydrogen. Additionally, small amounts of NH_3 are also released by all the samples.

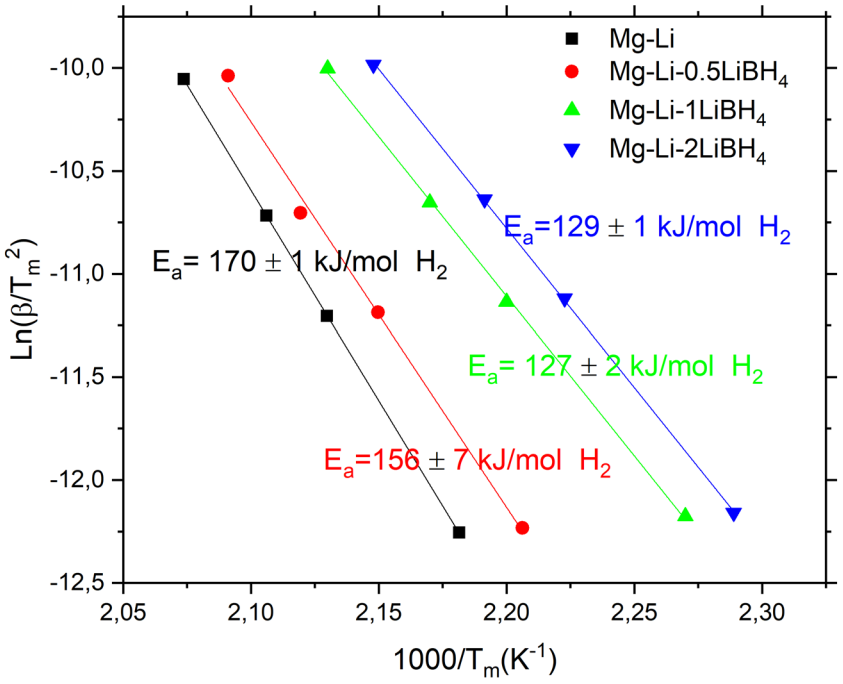

Figure 2 − Kissinger plots of as-milled samples derived from DSC curves at different heating rates (1, 3, 5 and 10 ºC/min) for the calculation of the apparent activation energies.

In order to evaluate the effect of the addition of $LiBH_4$ on the dehydrogenation kinetic behaviour of the Mg-Li composite, apparent activation energies (E_a) were calculated from DSC measurements by applying the Kissinger method. Figure 2 shows the resulting from Kissinger plots. All DSC curves along with the linear fitting for all the samples are shown in ESI: Figure S3. The apparent activation energy measured for the dehydrogenation of sample Mg-Li was found to be 170 ± 1 kJ/mol H_2. The activation energies reported in literature for the dehydrogenation of Li-Mg-N-H system are very diverse and range between 102 and 180 kJ/mol H_2 [43,62]. These variations can be attributed to different experimental conditions, i.e. gas flows, atmosphere, type of device and sample holder, as well as intrinsic parameters of the sample such as particle sizes, degree of mixture of reactants, crystal defects, among others. Reducing the particle size of $Mg(NH_2)_2$ + 2LiH system from 2 μm to 100 nm, the dehydrogenation E_a can be decreased from

182 to 122 kJ/mol. [54] Introducing $LiBH_4$ has also an effect on the decrease of the E_a. For the Mg-Li-0.5$LiBH_4$ sample, E_a is lowered to 156 ± 7 kJ/mol. A further reduction in the activation energy is observed for the samples Mg-Li-1$LiBH_4$ and Mg-Li-2$LiBH_4$, where E_a amounts 127 ± 2 kJ/mol and 129 ± 1 kJ/mol, respectively. This represents 24 % of reduction in the E_a compared to $LiBH_4$-free sample, which is in good agreement with literature [63].

3.2 First isothermal dehydrogenation/hydrogenation and characterization

The dehydrogenation/hydrogenation curves measured during the 1st cycle for all the samples are presented in Figure 3. It is clear that the addition of $LiBH_4$ improves the material kinetic behaviour. In 20 minutes, Mg-Li sample dehydrogenates only ~ 1.1 wt. % of H_2. During the same period of time, all other samples release more than 3 wt. % of H_2. Improvements in the absorption reaction kinetics are more significant. Within 10 minutes, Mg-Li-0.5$LiBH_4$, Mg-Li-1$LiBH_4$ and Mg-Li-2$LiBH_4$ samples absorb nearly 3.7 wt. %, 3.6 wt. % and 3.1 wt. % of H_2, respectively. Whereas, Mg-Li sample absorbs only ~ 1.4 wt. % of H_2 during the same period of time.

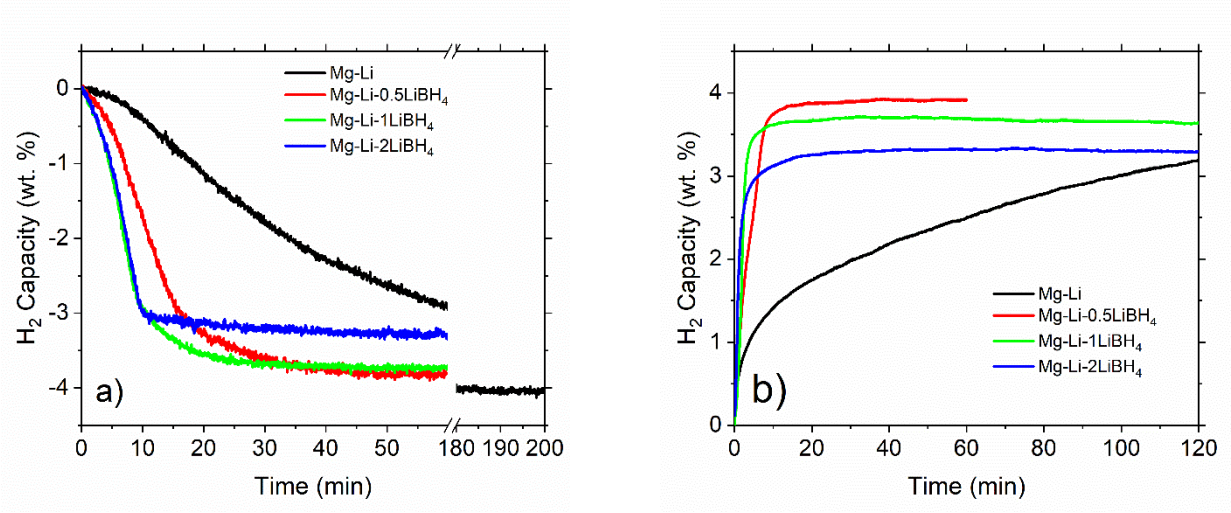

Figure 3 − (a) 1st isothermal dehydrogenation kinetics of as-milled samples at 180 °C and 1 bar of H_2 pressure. (b) 1st isothermal hydrogenation kinetics at 180 °C and 80 bar of H_2 pressure

In order to identify crystalline and non-crystalline phases present in the investigated samples, PXD and FT-IR measurements were performed, respectively. The PXD characterization of samples after 1st dehydrogenation at 180 °C are presented in Figure 4 (a). The diffraction peaks belonging to $Li_4(BH_4)(NH_2)_3$ are identified in the diffraction patterns of samples Mg-Li-0.5$LiBH_4$, Mg-Li-1$LiBH_4$ and Mg-Li-2$LiBH_4$. The characteristic diffraction peaks of $Li_2Mg_2(NH)_3$ are noted in all samples. In the diffraction pattern of Mg-Li, a broad peak around 2θ=51° is visible. On the contrary, such a broad peak is not present in the other diffraction patterns. The broad peak observed in the pattern of Mg-Li can be attributed to the presence of $Li_2Mg(NH)_2$. FT-IR spectra were measured between 500 and 4000 cm^{-1}. However, for the sake of clarity and to explain the reaction mechanism, we focus on the range between 3000 and 3500 cm^{-1}. It is worth mentioning that in the spectra of the $LiBH_4$ containing materials B-H stretching modes are detected between 2000 and 2500 cm^{-1} (not shown). As observed in the FT-IR spectrum of Mg-Li (Figure 4 (b)), the N-H stretching vibrations of $Li_2Mg(NH)_2$ fall at about 3174 cm^{-1}. However since the peak is very broad, it might also be attributed to a mixture of $Li_2Mg(NH)_2$ and $Li_2Mg_2(NH)_3$.

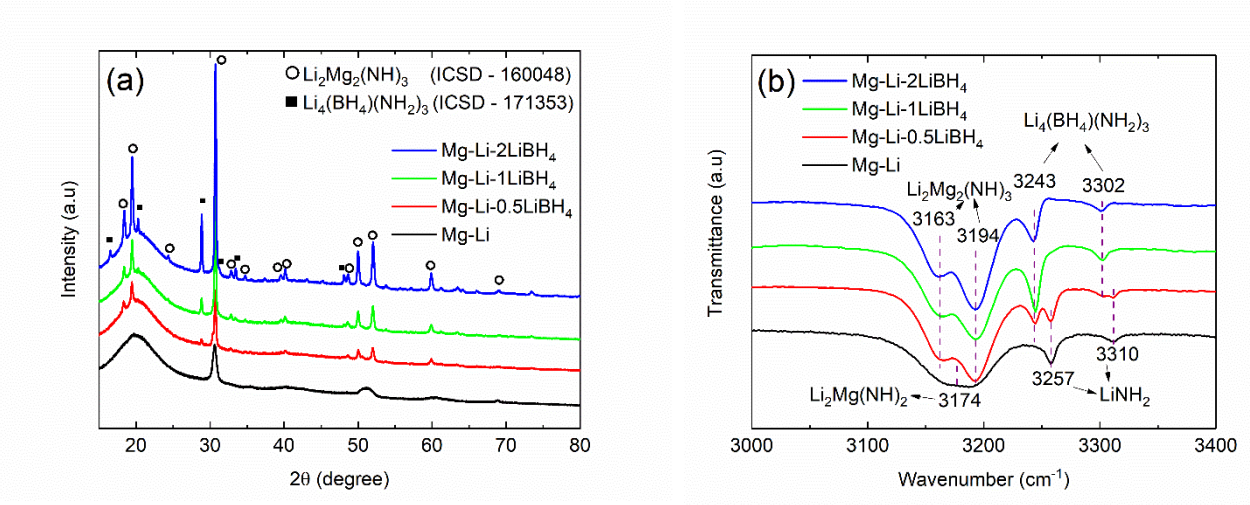

Figure 4 − (a) XRD patterns and (b) FT-IR spectra for samples after the first dehydrogenation at 180 °C and 1 bar of H_2.

The FT-IR spectrum acquired for Mg-Li sample shows two different absorption bands at 3257 cm^{-1} and 3310 cm^{-1}. These signals are related to the N–H stretching of $LiNH_2$. Interestingly, for sample Mg-Li-0.5$LiBH_4$, in addition to signal of the $LiNH_2$, N–H stretching modes from $Li_4(BH_4)(NH_2)_3$ at wavenumbers 3243 cm^{-1} and 3302 cm^{-1} are also observed. This suggests that the amount of $LiBH_4$ in Mg-Li-0.5$LiBH_4$ is not enough to react with all $LiNH_2$. When the amount of $LiBH_4$ is further increased, as in the case of Mg-Li-1$LiBH_4$ and Mg-Li-2$LiBH_4$, the typical absorption bands of $LiNH_2$ disappeared. This fact could be attributed to the formation of $Li_4(BH_4)(NH_2)_3$ from the interaction between $LiNH_2$ and $LiBH_4$ during dehydrogenation as previously reported in the literature [60].

The Mg-Li sample presents two overlapped dehydrogenation thermal events (Figure 1) and its characterization after the first dehydrogenation along with its reversible capacity evidences that the sample reversibly store hydrogen following reactions 2 and 3. dehydrogenation/hydrogenation processes for all samples are reversible, since the overall H_2 capacities are kept constant. For the samples containing $LiBH_4$, the reaction pathways are clearly different. On the one hand, the Mg-Li-0.5$LiBH_4$ sample gives $LiNH_2$, $Li_4(BH_4)(NH_2)_3$ and $Li_2Mg_2(NH)_3$ as dehydrogenation products (Figure 4 (b)), following the reaction 5

$$6Mg(NH_2)_2 + 9LiH + 0.5LiBH_4 \leftrightharpoons 3Li_2Mg_2(NH)_3 + 1.5LiNH_2 + 0.5Li_4(BH_4)(NH_2)_3 + 9H_2 \quad (5)$$

On the other hand, $LiNH_2$ is not present in the Mg-Li-1$LiBH_4$ and Mg-Li-2$LiBH_4$ samples. The main dehydrogenation products are $Li_2Mg_2(NH)_3$, $Li_4(BH_4)(NH_2)_3$ and $Li_2(BH_4)(NH_2)$, following reactions 6 and 7. In a previous work, the formation of $Li_2(BH_4)(NH_2)$ during the dehydrogenation reactions of Li-Mg-B-N-H system was shown [46]. This phase is present at the beginning of dehydrogenation and transforms into $Li_4(BH_4)(NH_2)_3$ and $LiBH_4$ in the later stage [46]. Since we

focused on the characterization of the samples after dehydrogenation, it is possible that this intermediate already transformed into $Li_4(BH_4)(NH_2)_3$.

$$6Mg(NH_2)_2 + 9LiH + 1LiBH_4 \leftrightharpoons 3Li_2Mg_2(NH)_3 + Li_4(BH_4)(NH_2)_3 + 9H_2 \quad (6)$$

$$6Mg(NH_2)_2 + 9LiH + 2LiBH_4 \leftrightharpoons 3Li_2Mg_2(NH)_3 + Li_4(BH_4)(NH_2)_3 + LiBH_4 + 9H_2 \quad (7)$$

3.3 Cycling behaviour for the Li-Mg-N-H and Li-Mg-N-B-H systems

Twenty dehydrogenation/hydrogenation cycles were performed for all the as-milled samples isothermally at 180 °C (kinetic curves ESI – Figure S4). Measured gravimetric H_2 capacities and

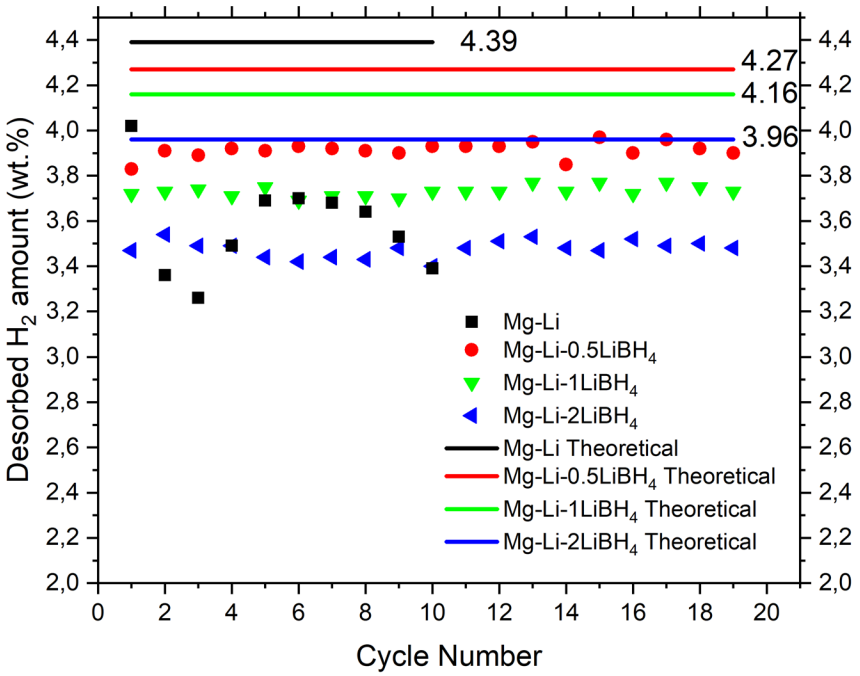

Figure 5 − Desorbed H_2 amounts from the samples for the first 20 isothermal dehydrogenation cycles (180 °C and 1 bar of H_2 pressure). Mg-Li sample was cycled 10 times due to long measurement time.

cycling stabilities for all the investigated systems over the 20th cycles are reported in Figure 5. The amount of desorbed H_2 is reduced from 4.0 wt. % to 3.6 wt. % within 10 cycles for Mg-Li, even if the measurement time is extended. Mg-Li-0.5$LiBH_4$ sample desorbs ~ 3.9 wt. of H_2 over 20 cycles. H_2 storage capacities reduce to ~ 3.7 wt. % and 3.5 wt. % for Mg-Li-1$LiBH_4$ and Mg-Li-2$LiBH_4$ samples, respectively. All $LiBH_4$-containing samples exhibit excellent cycling stabilities with no detectable capacity drop as reported in a previous work [44].

The diffraction patterns acquired for the material after 20 cycles are presented in ESI Figure S5. This figure clearly shows that for the chosen operating conditions no crystalline side-products are formed. The experimentally measured gravimetric H_2 capacities are in accordance with the theoretical ones for all samples.

In order to compare hydrogenation and dehydrogenation kinetic behaviour for all the studied systems upon cycling, the absorption and desorption times necessary to achieve the 80 % of the hydrogen storage capacity was taken into consideration. The collected results are summarized in Figure 6. In the first cycle of sample Mg-Li, dehydrogenation and hydrogenation times necessary to achieve 80 % of the maximum capacity are 70 and 63 minutes, respectively. $LiBH_4$ helps significantly to improve the kinetic behaviour, since H_2 desorption and absorption times in the first cycle take just 17 and 6 minutes for Mg-Li-0.5$LiBH_4$ sample, respectively. This values are ~ 4 and ~ 10 times faster of the dehydrogenation and hydrogenation processes of Mg-Li. A further improvement is observed when the amount of additive is increased in the composite. For Mg-Li-1$LiBH_4$ and Mg-Li-2$LiBH_4$ samples, dehydrogenation and hydrogenation times are achieved in about 10 minutes and 3 minutes, respectively. These times are increased in the following cycles for all samples except for Mg-Li-2$LiBH_4$, which has the highest amount of additive. An increase

in the H_2 absorption and desorption characteristic times between the 1st and the 19th cycle is only about 1 minute for the Mg-Li-2LiBH4 sample. Therefore, Mg-Li-2LiBH4 has potential for further investigation at larger scale due to stable reaction kinetics over 20 reaction cycles, excellent cycling stability and gravimetric capacity of about 3.5 wt. % H_2.

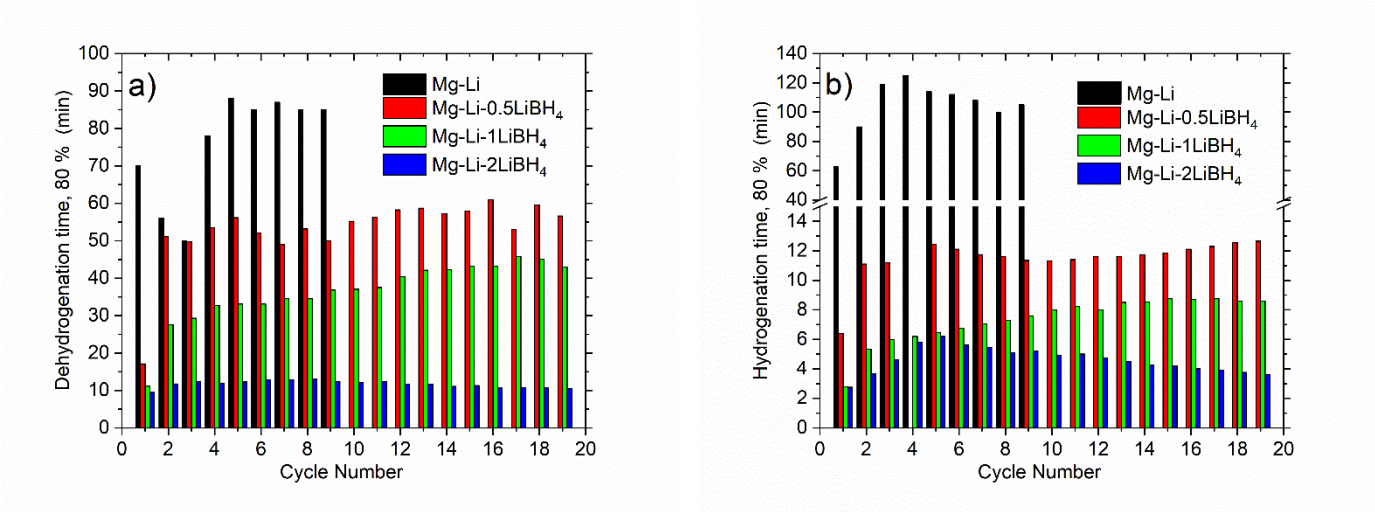

Figure 6 − Times to reach 80 % of the (a) dehydrogenation and (b) hydrogenation capacities over 20 cycles

3.4 Evaluation of the rate-limiting step upon cycling

In previous works, the reaction mechanism of Li-Mg-N-H system has been studied [64–66]. From these studies, it emerges that the mass transport of small ions (e.g., Li^+, Mg^{+2}, and H^+) during dehydrogenation as well as the reactions at the interfaces of amide and hydrides play a crucial role in determining the overall kinetic properties of the material. Matsuo *et al.* showed that the Li^+ conductivity of $Li_4(BH_4)(NH_2)_3$ is 4 and 5 orders of magnitude higher than that of $LiBH_4$ and $LiNH_2$, respectively [48]. Cao *et al.* suggested the possible existence of a "liquid like" state of $Li_4(BH_4)(NH_2)_3$ based on *in-situ* synchrotron XRD evidences [67]. In these experiments, it is observed that the diffraction peaks of $Li_4(BH_4)(NH_2)_3$ disappear at temperatures of ~ 180 °C

because it might have melted. It was proposed that the formation of $Li_4(BH_4)(NH_2)_3$ weakens the N-H bonds, improving the reversibility of the amide-imide phase transformations [68].

In order to gain understanding about the intrinsic kinetic constraints for the hydrogenation and dehydrogenation upon cycling, solid-state models were applied to the 1st and 9th dehydrogenation/hydrogenation cycles for the samples showing different reaction pathways, i.e. Mg-Li, Mg-Li-0.5$LiBH_4$ and Mg-Li-2$LiBH_4$. This is the first time that such intensive analysis is carried out with this tri-component system, to the best of our knowledge. The results from the fittings are listed in Table 2. All the fitting details are shown in ESI Figures S6-S11 and Tables S2-S13.

Table 2 − Rate-limiting processes of samples, which were defined from isothermal reaction curves with Sharp and Jones method [57, 58]

Sample code	**Dehydrogenation**		**Hydrogenation**	
	1st	**9th**	**1st**	**9th**
Mg-Li	R3	D1	D3	D3
Mg-Li-0.5$LiBH_4$	F2	D1	R3	R3
Mg-Li-2$LiBH_4$	F2	F2	F1	F1

R3 : Three-dimensional growth of contracting volume with constant interface velocity

D1 : One-dimensional diffusion

D3 : Three-dimensional diffusion

F1 : JMA, n = 1, Random nucleation, one-dimensional interface controlled growth

F2 : JMA, n = 1/2, Random nucleation, one-dimensional diffusion with constant number of nuclei

In the case of the dehydrogenation kinetic behaviour, it is possible to see that the rate-limiting steps are different when the sample contains $LiBH_4$ (Table 2). During the first cycle, the Mg-Li sample is controlled by interface mechanism, while all the $LiBH_4$ –containing samples present diffusion controlled mechanism (F2).

For the pristine sample Mg-Li, R3-model suggests that the reaction rate during the first dehydrogenation is controlled by the reactions occurring at the interfaces (ESI Figure S4 (a_1)), in agreement with previously reported work [69]. Independent on the concentration of $LiBH_4$, best fitting for all $LiBH_4$-containing samples was obtained with F2 diffusion controlled model. Compared to Mg-Li, these samples have faster dehydrogenation kinetics during the first dehydrogenation (ESI Figure S4 (a_1- c_1)). It is clear that the reaction pathway for the $LiBH_4$-containing samples are different from the pristine one. In the presence of $LiBH_4$, more stable dehydrogenation products are obtained at the amide-imide interfaces by exothermic reaction of $LiNH_2$ and $LiBH_4$ to form $Li_4(BH_4)(NH_2)_3$. Hence, the diffusion processes required for the formation of intermediate species, as indicated in reactions 5-7, account for the change in the mechanism, i.e. from R3 (Mg-Li) to F2.

At the ninth dehydrogenation, reaction rates of Mg-Li and Mg-Li-0.5$LiBH_4$ samples show D1 diffusion model as rate-limiting step. It is noteworthy that the dehydrogenation kinetic of Mg-Li-0.5$LiBH_4$ sample significantly slows down after cycling (ESI Figure S4 (b_1)). It is possible to see that the rate-limiting step for Mg-Li-0.5$LiBH_4$ is the same as for the pristine one. Poor kinetic properties after adding small amount of $LiBH_4$ can be attributed to the agglomeration and phase separation within the sample, occurring at relatively high operating temperature condition (180 °C). It was reported before that this is a general problem for the Li-Mg-N-H system [70,71]. For the Mg-Li-2$LiBH_4$, instead, the rate-limiting step does not change after cycling (F2). This sample

maintain its fast dehydrogenation kinetics over 20 cycles (ESI Figure S4 (c_1)). Adding more $LiBH_4$ facilitates the formation of $Li_4(BH_4)(NH_2)_3$ and $Li_2(BH_4)(NH_2)$ as shown in reaction 7. However, based on the analysis through the gas-solid models, herein, it is proposed that the kinetic constraints come mainly from the solid-solid diffusion processes of the species to form $Li_4(BH_4)(NH_2)_3$ and $Li_2(BH_4)(NH_2)$.

First hydrogenation kinetic behaviour of samples show that depending on the $LiBH_4$ stoichiometry, the rate-limiting steps change (Table 2). Reaction-rate of the Mg-Li sample is controlled by three-dimensional diffusion (D3) model. This kind of controlled mechanism during the hydrogenation usually occur for several hydrogen forming materials [72]. Considering that the Mg-Li is a multi-component system, it is possible to relate the diffusion-controlled mechanism to the slow mobility of the species upon hydrogenation. Mg-Li-0.5$LiBH_4$ and Mg-Li-2$LiBH_4$ sample show interface controlled mechanisms (R3 and F1). Hydrogenation kinetics of these samples are much faster than the one of Mg-Li sample (ESI Figure S4 (a_2-c_2)). The faster hydrogenation rates, the reaction pathways and the rate-limiting step models, suggest that the enhancement of the kinetic behaviour (ESI Figure S4 (b2, c2)) can be attributed to the presence of highly ionic species as shown in reactions 5 and 7. At the ninth hydrogenation, the rate-limiting steps do not change for any of the samples compared to the first hydrogenation, which is in agreement with the slightly changes observed for the hydrogenation curves.

Summarizing, based on the above mentioned analysis along with the literature and our results from volumetric measurements and characterizations (DSC, FT-IR, PXD), it is possible to propose that the exothermic reaction between $LiNH_2$ and $LiBH_4$ to form $Li_4(BH_4)(NH_2)_3$ or $Li_2(BH_4)(NH_2)$ during the first dehydrogenation accelerates the reaction rates at the amide-imide phase

boundaries. In the case of hydrogenation, highly ionic conductive $Li_4(BH_4)(NH_2)_3$ can assist the diffusion of small ions into the interfaces of the amide-hydride matrix.

4 Conclusion

Compositional effects of $LiBH_4$ on the $6Mg(NH_2)_2$-9LiH system show noticeable improvement in the apparent activation energies, reaction kinetics and cycling stability. Increasing the amount of $LiBH_4$ in the composite results in lowered apparent dehydrogenation activation energies (170 kJ/mol H_2 for Mg-Li and 129 kJ/mol H_2 for Mg-Li-2$LiBH_4$). During the dehydrogenation, reactions between $LiNH_2$ and $LiBH_4$ to form $Li_4(BH_4)(NH_2)_3$ accelerate the kinetic behaviour at the interfaces of amide-hydride particles, which leads to a change in the interface-controlled mechanism to diffusion controlled mechanism. During the hydrogenation, highly ionic conductive $Li_4(BH_4)(NH_2)_3$ can assist the diffusion of small ions into the interfaces of the amide-hydride matrix. To the best of our knowledge, such intensive analysis regarding the cycling properties and reaction mechanism were performed for the first time. This research provides detailed information about the kinetic behaviour and reaction mechanism on the Li-Mg-B-N-H system and presents Mg-Li-2$LiBH_4$ as a material with interesting properties for hydrogen storage applications.

5 Conflicts of Interest

The authors declare that there is no conflict of interest regarding the publication of this article.

6 Funding Statement

This work was supported by the CAS-HZG collaborative project ‘‘RevHy’’ – ‘‘Study on the synthesis, structures and performances of complex hydrides systems for Reversible high capacity Hydrogen storage at low temperatures’’.

The authors thank CONICET (Consejo Nacional de Invetigaciones Científicas y Técnicas) and Alexander von Humboldt Foundation in the frame of the post-doctoral fellowship of Dr. J. Puszkiel (Fellowship number: ARG - 1187279 - GF - P).

7 Author Information

Corresponding Authors;

1. Claudio Pistidda, E-mail: Claudio.pistidda@hzg.de
2. Martin Dornheim, E-mail: Martin.dornheim@hzg.de

8 References

[1] KYOTO Protocol to the United Nations Framework Convention on Climate Change, *United Nations*. **1998**.

[2] Global Energy Transformation: A roadmap to 2050, *International Renewable Energy Agency*. **2018.**

[3] Renewables 2017 Global Status Report. *REN21*. **2017**.

[4] White Paper on transport — Roadmap to a single European transport area — Towards a competitive and resource-efficient transport system. *European Commission*. **2011**. DOI:10.2832/30955.

[5] Schlapbach, L.; Züttel, A. Hydrogen-storage materials for mobile applications. *Nature.* **2001**, 414, 353–358. DOI:10.1038/35104634

[6] Züttel, A. Materials for hydrogen storage. *Mater. Today*. **2003,** 6**,** 24–33. DOI: 10.1016/S1369-7021(03)00922-2

[7] Milanese, C.; Garroni, S.; Gennari, F.; Marini, A.; Klassen, T. Solid State Hydrogen Storage in Alanates and Alanate-Based Compounds: A Review. *Metals.* **2018**, 8, 567. DOI:10.3390/met8080567

[8] A. Puszkiel, J.; Garroni, S.; Milanese, C.; Gennari, F.; Klassen, T. Tetrahydroborates: Development and Potential as Hydrogen Storage Medium. *Inorganics.* **2017**, 5, 74. DOI:10.3390/inorganics5040074

[9] Garroni, S.; Santoru, A.; Cao, H.; Dornheim, M; Klassen, M. Recent Progress and New Perspectives on Metal Amide and Imide Systems for Solid-State Hydrogen Stroage. **2018**, 11, 1027. DOI:10.3390/en11051027

[10] Bellosta Von Colbe, J.; Lonzano, G.; Metz, O.; Bücherl, T.; Bormann, R. Design, sorption behaviour and energy management in a sodium alanate-based lightweight hydrogen storage tank. *Int. J. Hydrogen Energy*. **2015**, 40, 7. DOI:10.1016/j.ijhydene.2015.01.013

[11] Santoru, A.; Pistidda, C.; Brighi, M.; R. Chierotti, M.; Heere, M. Insights into the Rb − Mg − N − H System: an Ordered Mixed Amide/Imide Phase and a Disordered Amide/Hydride Solid Solution. *Inorganic Chemistry.* **2018**, 57, 3197−3205. DOI:10.1021/acs.inorgchem.7b03232

[12] Capurso, G.; Schiavo, B.; Jepsen, J.; A. Lozano, G.; Metz, O. Metal Hydride-Based Hydrogen Storage Tank Coupled with an Urban Concept Fuel Cell Vehicle : Off Board Tests. *Advanced Sustainable Systems.* **2018**, 1800004. DOI:10.1002/adsu.201800004

[13] Jepsen, J.; Milanese, C.; A. Puszkiel, J.; Girella, A.; Schiavo, B. Fundamental material properties of the $2LiBH_4$-MgH_2 Reactive Hydride Composite for Hydrogen Storage: (I) Thermodynamic and Heat Transfer Properties. *Energies*. **2018**, 11(5), 1081. DOI:10.3390/en11051081

[14] Karimi, F.; Pranzas K.; Pistidda, C.; A. Puskiel, J.; Milanese, C. Structural and kinetic investigation of the hydride composite $Ca(BH_4)_2$ + MgH_2 system doped with NbF_5 for solid-state hydrogen storage. *Phys. Chem. Chem. Phys.* **2015**, 17, 27328-27342. DOI:10.1039/c5cp03557k

[15] Bergemann, N.; Pistidda, C.; Milanese, C.; Emmler, T.; Karimi, F. $Ca(BH_4)_2$-Mg_2NiH_4: On the pathway to a $Ca(BH_4)_2$ system with a reversible hydrogen cycle. *Chem. Commun.* **2016**, 52, 4836–4839. DOI: 10.1039/C5CC09991A

[16] Chaudhary, A. L.; Li, G.; Matsuo, M.; Orimo, S. I.; Deledda, S. Simultaneous desorption behavior of M borohydrides and Mg_2FeH_6 reactive hydride composites (M = Mg, then Li, Na, K, Ca). *Appl. Phys. Lett.* **2015**, 107, 7. DOI:10.1063/1.4929340

[17] Pireddu G.; Valentoni A,; Bonatto Minella C,; Pistidda C. Comparison of the thermochemical and mechanochemical transformations in the $2NaNH_2$-MgH_2 system. *Int. J. Hydrogen Energy*. **2015**, 40, 4, 1829–1835. DOI:10.1016/j.ijhydene.2014.11.145

[18] Milanese, C; Jensen, T. R.; Hauback, B. C.; Pistidda, C. Complex hydrides for energy

storage, *Int. J. Hydrogen Energy*. **2019**, In press, corrected proof. DOI:10.1016/j.ijhydene.2018.11.208

[19] Jose Bellosta von Colbe, Jose-Ramon Ares , Jussara Baralei, Marcello Baricco, Craig Buckley, Application of hydrides in hydrogen storage and compression: Achievements, outlook and perspectives, *Int. J. Hydrogen Energy*. **2019**, In press, corrected proof. DOI:10.1016/j.ijhydene.2019.01.104

[20] Z. Pei, Y. Bai, Y. Wang, F. Wu, and C. Wu. Insight to the Thermal Decomposition and Hydrogen Desorption Behaviors of $NaNH_2$-$NaBH_4$ Hydrogen Storage Composite. *ACS Appl. Mater. Interfaces*. **2017**, 9, 37, 31977–31984. DOI:10.1021/acsami.7b10043

[21] Y. Bai, C. Wu, F. Wu, J. Yang, L. Zhao. Thermal decomposition kinetics of light-weight composite $NaNH_2$-$NaBH_4$ hydrogen storage materials for fuel cells. *Int. J. Hydrogen Energy*. **2012**, 37, 17, 12973–12979. DOI:10.1016/j.ijhydene.2012.05.069

[22] J. L. Gay-Lussac; L. J. Thenard. Notiz über das Kali - und das Natron - Metall. *Annalen der Physik*. **1809**, 32, 23-39

[23] F. W. Dafert; R. Miklauz. Über einige neue Verbindungen von Stickstoff und Wasserstoff mit Lithium. *Manotsh chem*. **1910**, 31, 981-996

[24] R. Juza; K. Opp. Zur Kenntnis des Lithiumimides. *Z. anorg. allg. Chem. 268,*. **1951**, 266, 313.

[25] M. Schütze. Introduction to High Temperature Oxidation and Corrosion. *Materials and Corrosion*. **2003**, 54, 5, 346-347. DOI:10.1002/maco.200390081

[26] Chen, P.; Xiong, Z.; Luo, J.; Lin, J; Lee Tan, K. Interaction of hydrogen with metal nitrides and imides. *Nature*. **2002**, 420. DOI:10.1038/nature01210

[27] Luo, W.; Rönnebro, E. Towards a viable hydrogen storage system for transportation application. *J. Alloys Compd.* **2005**, 404–406**,** 392–395. DOI:10.1016/j.jallcom.2005.01.131

[28] Leng, H. Y.; Ichikawa, T.; Hino, S.; Hanada, N.; Isobe, S. New Metal-N-H system composed of $Mg(NH_2)_2$ and LiH for hydrogen storage. *J. Phys. Chem. B.* **2004**, 108, 8763-8765. DOI:10.1021/jp048002j

[29] Xiong, Z.; Wu, G.; Hu, J.; Chen, P. Ternary imides for hydrogen storage. *Adv. Mater.* **2004**, 16, 17. DOI:10.1002/adma.200400571

[30] Xiong, Z.; Wu, G.; Hu, J.; Liu, Y.; Chen, P. Reversible Hydrogen Storage by a Li–Al–N–H Complex. *Adv. Funct. Mater.* **2007**, 17, 1137–1142. DOI: 10.1002/adfm.200600759

[31] Torre, F.; Valentoni, A.; Milanese, C.; Pistidda, C.; Marini, A. Kinetic improvement on the CaH_2-catalyzed $Mg(NH_2)_2$ + 2LiH system. *Journal of Alloys and Compounds*. **2014**, 645, 1, S284-S287. DOI:10.1016/j.jallcom.2014.12.228

[32] Zhu, X.; Han, S.; Zhao, X.; Li, Y.; Liu, B. Effect of lanthanum hydride on microstructures and hydrogen storage performances of $2LiNH_2$-MgH_2 system. *J. Rare Earths*. **2014**, 32, 5, 429. DOI:10.1016/S1002-0721(14)60089-2

[33] Zhang, Y.; Xiong, Z.; Cao, H.; Wu, G.; Chen, P. The enhanced hydrogen storage performance of (Mg-B-N-H)-doped $Mg(NH_2)_2$-2LiH system. *Int. J. Hydrogen Energy* **2014**, 39, 4, 1710-1718. DOI:10.1016/j.ijhydene.2013.11.008

[34] Amica, G.; Enzo, S.; Larochette, P. A.; Gennari, F. C. Improvements in the hydrogen storage properties of the $Mg(NH_2)_2$ –LiH composite by KOH addition. *Phys. Chem. Chem. Phys.* **2018**, 20, 15358-15367. DOI:10.1039/c8cp02347f

[35] Liang, C.; Liu, Y.; Wei, Z.; Jiang, Y.; Gao, M. Enhanced dehydrogenation/hydrogenation kinetics of the $Mg(NH_2)_2$-2LiH system with NaOH additive. *Int. J. Hydrogen Energy*. **2011**, 36, 3, 2137-2144. DOI:10.1016/j.ijhydene.2010.11.068

[36] Wang, J.; Liu, T.; Wu, G.; Li, W.; Liu, Y. Potassium-Modified $Mg(NH_2)_2$/2LiH System for Hydrogen Storage. *Angew. Chem.* **2009**, 48, 32, 5828-5832. DOI:10.1002/anie.200805264

[37] Wang, J.; Chen, P.; Pan, H.; Xiong, Z.; Gao, M. Solid–Solid Heterogeneous Catalysis: The Role of Potassium in Promoting the Dehydrogenation of the $Mg(NH_2)_2$/2LiH Composite. *Chemsuschem*. **2013**, 6, 2181-2189. DOI:10.1002/cssc.201200885

[38] Li, C.; Liu, Y.; Gu, Y.; Gao, M.; Pan, H. Improved hydrogen-storage thermodynamics and kinetics for an RbF-doped $Mg(NH_2)_2$-2 LiH system. *Chem. - An Asian J.* **2013**, 8, 2136–2143. DOI: 10.1002/asia.201300323

[39] Li, C.; Liu, Y.; Ma, R.; Zhang, X.; Li, Y. Superior dehydrogenation/hydrogenation kinetics and long-term cycling performance of K and Rb Cocatalyzed $Mg(NH_2)_2$-2LiH system. *ACS Appl. Mater. Interfaces*. **2014**, 6, 17024−17033. DOI:10.1021/am504592x

[40] Li, B.; Liu, Y.; Gu, J.; Gu, Y.; Gao, M. Mechanistic investigations on significantly improved hydrogen storage performance of the $Ca(BH_4)_2$-added $2LiNH_2/MgH_2$ system. *Int. J. Hydrogen Energy.* **2013**, 38, 12, 5030–5038. DOI:10.1016/j.ijhydene.2013.02.011

[41] Pan, H.; Shi, S.; Liu, Y.; Li, B.; Yang, Y. Improved hydrogen storage kinetics of the Li-Mg-N-H system by addition of $Mg(BH_4)_2$. *Dalt. Trans.* **2013**, 42, 3802. DOI:10.1039/c2dt32266h.

[42] Hu, J.; Liu, Y.; Wu, G.; Xiong, Z.; Chua, Y. S. Improvement of Hydrogen Storage Properties of the Li–Mg–N–H System by Addition of $LiBH_4$. *Chem. Mater*. **2008**, 20, 4398-4402. DOI:10.1021/cm800584x

[43] Xiong, Z.; Hu, J.; Wu, G.; Chen, P.; Luo, W. Thermodynamic and kinetic investigations of the hydrogen storage in the Li-Mg-N-H system. *J. Alloys Compd.* **2005**, 398, 235-239. DOI:10.1016/j.jallcom.2005.02.010

[44] Cao, H.; Wu, G.; Zhang, Y.; Xiong, Z. Qiu, J. Effective thermodynamic alteration to $Mg(NH_2)_2$-LiH system: Achieving near ambient-temperature hydrogen storage. *J. Mater. Chem. A*. **2014**, 2, 15816. DOI:10.1039/c4ta03505d

[45] Lewis, G. J.; Sachtler, J. W. A.; Low, J. J.; Lesch, D. A.; Faheem, S. A. High throughput screening of the ternary $LiNH_2$-MgH_2-$LiBH_4$ phase diagram. *J. Alloys Compd.* **2007**, 446–447**,** 355–359. DOI:10.1016/j.jallcom.2007.04.028

[46] Wang, H.; Cao, H.; Wu, G.; He, T.; Chen, P. The improved hydrogen storage performances of the multi-component composite: $2Mg(NH_2)_2$-3LiH-$LiBH_4$. *Energies* **2015**, 8, 6898–6909. DOI:10.3390/en8076898

[47] Meisner, G. P.; Scullin, M. L.; Balogh, M. P.; Pinkerton, F. E; Meyer, M. S. Hydrogen release from mixtures of lithium borohydride and lithium amide: A phase diagram study. *J. Phys. Chem. B.* **2006**, 110, 4186-4192. DOI:10.1021/jp056019b

[48] Matsuo, M.; Remhof, A.; Martelli, P.; Caputo, R.; Ernst, M. Complex Hydrides with $(BH_4)^-$ and $(NH_2)^-$ Anions as New Lithium Fast-Ion Conductors. *J. AM. CHEM. SOC.* **2009**, 131, 16389–16391. DOI:10.1021/ja907249p

[49] Wang, Z.; Lijung, J.; Yuanfang, W.; Jianhua, Y.; Baolong, Y. Improved dehydrogenation cycle performance of the $1.1MgH_2$-$2LiNH_2$-$0.1LiBH_4$ system by addition of $LaNi_{4.5}Mn_{0.5}$ alloy. *J. Rare Earths.* **2015,** 33, 7, 783–790. DOI:10.1016/S1002-0721(14)60485-3

[50] Hu, J.; Pohl, A.; Wang, S.; Rothe, J.; Fichtner, M. Additive Effects of $LiBH_4$ and $ZrCoH_3$ on the Hydrogen Sorption of the Li-Mg-N-H Hydrogen Storage System. *J. Phys. Chem. C* **2012**, 116, 20246–20253. DOI:10.1021/jp307775d

[51] Shukla, V.; Bhatnagar, A.; Soni, P. K.; Vishwakarma, A. K.; Shaz, M. A. Enhanced hydrogen sorption in a Li–Mg–N–H system by the synergistic role of $Li_4(NH_2)_3BH_4$ and $ZrFe_2$. *Phys. Chem. Chem. Phys*. **2017**, 19, 9444–9456. DOI:10.1039/c6cp08333a

[52] Gutfleisch, O. High pressure milling vial Gas-Temperature-Monitoring System. Evico Magnetics. **2007**

[53] Takeo Ozawa, Kinetic analysis by repeated temperature scanning. Part 1. Theory and methods, *Thermochimica Acta*. **2000**, 356, 173-180. DOI: 10.1016/S0040-6031(00)00517-7

[54] Kissinger, H. E. Reaction Kinetics in Differential Thermal Analysis. *Analytical Chemistry*. **1957**, 29, 11, 1702–1706.

[55] P. M. Madhusudanan, K. Krishnan, and K. N. Ninan. New approximation for the p(x) function in the evaluation of non-isothermal kinetic data. *Thermochim. Acta*. **1986**, 97, 189-201

[56] Coats AW, Redfern JP. Kinetic parameters from thermogravimetric data. *Nature*. **1964**, 210, 68-9

[57] Sharp, J. H.; Brindley, G. W.; Achar, B. N. N. Numerical Data for Some Commonly Used Solid State Reaction Equations. *J. Am. Ceram. Soc.* **1966**, 49, 7, 379-383.

[58] Jones, L. F.; Dollimore, D.; Nicklin, T. Comparison of experimental kinetic decomposition data with master data using a linear plot method. *Thermochim. Acta* **1975**, 13, 240–245.

[59] Bergerhoff, G.; Brown, I. D. i. Crystallographic Databases (ICSD). *International Union of Crystallography*. **1987**, F.H. Allen et al. (Hrsg.) Chester.

[60] Hu, J.; Weidner, E.; Hoelzel, M.; Fichtner, M. Functions of $LiBH_4$ in the hydrogen sorption reactions of the 2LiH-$Mg(NH_2)_2$ system. *Dalt. Trans*. **2010**, 39, 9100–9107. DOI:10.1039/c0dt00468e

[61] Fedneva, E.M.; Alpatova, V.I.; Mikheeva, V.I. Thermal Stability of Lithium Tetrahydrobarate. *Russian Journal of Inorganic Chemistry* **1964**, 9, 6:826–827

[62] Xie, L.; Liu, Y.; Li, G.; Li, X. Improving Hydrogen Sorption Kinetics of the $Mg(NH_2)_2$-LiH System by the Tuning Particle Size of the Amide. *J. Phys. Chem. C*. **2009**, 113, 14523–14527. DOI:10.1021/jp904346x

[63] Wang, H.; Cao, H.; Pistidda, C.; Garroni, S.; Wu, G. Effects of Stoichiometry on the H_2-Storage Properties of $Mg(NH_2)_2$–LiH–$LiBH_4$ Tri-Component Systems. *Chem. Asian J.* **2017**, 12, 1758 –1764. DOI:10.1002/asia.201700287

[64] Wang, J.; Li, H.; Wang, S.; Liu, X.; Li, Y. The desorption kinetics of the $Mg(NH_2)_2$ + LiH mixture. *Int. J. Hydrogen Energy*. **2009**, 34, 1411–1416. DOI:10.1016/j.ijhydene.2008.11.038

[65] Liu, Y.; Zhong, K.; Luo, K.; Gao, M.; Pan, H. Size-dependent kinetic enhancement in hydrogen absorption and desorption of the Li-Mg-N-H system. *J. Am. Chem. Soc*. **2009**, 131, 1862–1870. DOI:10.1021/ja806565t

[66] Nayebossadri, S. Kinetic rate-limiting steps in dehydrogenation of Li-N-H and Li-Mg-N-H systems - Effects of elemental Si and Al. *Int. J. Hydrogen Energy.* **2011**, 36, 8335-8343. DOI:10.1016/j.ijhydene.2011.03.169

[67] Cao, H.; Zhang, W.; Pistidda, C.; Puszkiel, J.; Milanese, C. Kinetic alteration of the $6Mg(NH_2)_2$–$9LiH$–$LiBH_4$ system by co-adding YCl_3 and Li_3N. *Phys. Chem. Chem. Phys*. **2017**, 19, 32105–32115. DOI: 10.1039/C7CP06826C

[68] Filinchuk, Y. E.; Yvon, K.; Meisner, G. P.; Pinkerton, F. E.; Balogh, M. P. On the composition and crystal structure of the new quaternary hydride phase $Li_4BN_3H_{10}$. *Inorg. Chem*. **2006,** 45, 1433–1435. DOI:10.1021/ic0518226

[69] Chen, P.; Xiong, Z.; Yang, L.; Wu, G.; Luo, W. Mechanistic investigations on the heterogeneous solid-state reaction of Magnesium Amides and Lithium Hydrides. *J. Phys. Chem. B*. **2006**, 110, 14221–14225. DOI:10.1021/jp061496v

[70] Cao, H.; Wang, H.; He, T.; Wu, G.; Xiong, Z. Improved kinetics of the $Mg(NH_2)_2$-2LiH system by addition of lithium halides. *RSC Adv*. **2014**, 4, 32555–32561. DOI:10.1039/c4ra02864c

[71] Yan, M. Y.; Sun, F.; Liu, X. P.; Ye, J. H.; Yuan, H.P. Experimental study on hydrogen storage properties of Li–Mg–N–H based tank. *J. Alloys Compd*. **2014**, 603, 19-22. DOI:10.1016/j.jallcom.2014.03.054

[72] Nurul, N. Z.; Yaakob, Z.; Lim, K. L.; Timmiati, S. N. The kinetics of lightweight solid-state hydrogen storage materials: A review. *Int. J. Hydrogen Energy*. **2016**, 41, 13131–13151. DOI:10.1016/j.ijhydene.2016.05.169